Nurul Amziah Md. Yunus[1]
Hossein Nili[2]
Nicolas G. Green[2]

[1]Department of Electrical and Electronic Engineering, Faculty of Engineering, Universiti Putra Malaysia, Selangor, Malaysia
[2]Nano Group, School of Electronics and Computer Science, University of Southampton, Highfield, Southampton, UK

Received August 24, 2012
Revised October 22, 2012
Accepted November 7, 2012

Research Article

Continuous separation of colloidal particles using dielectrophoresis

Dielectrophoresis is the movement of particles in nonuniform electric fields and has been of interest for application to manipulation and separation at and below the microscale. This technique has the advantages of being noninvasive, nondestructive, and noncontact, with the movement of particle achieved by means of electric fields generated by miniaturized electrodes and microfluidic systems. Although the majority of applications have been above the microscale, there is increasing interest in application to colloidal particles around a micron and smaller. This paper begins with a review of colloidal and nanoscale dielectrophoresis with specific attention paid to separation applications. An innovative design of integrated microelectrode array and its application to flow-through, continuous separation of colloidal particles is then presented. The details of the angled chevron microelectrode array and the test microfluidic system are then discussed. The variation in device operation with applied signal voltage is presented and discussed in terms of separation efficiency, demonstrating 99.9% separation of a mixture of colloidal latex spheres.

Keywords:
Colloidal / Dielectrophoresis / Separation DOI 10.1002/elps.201200466

1 Introduction

1.1 General

Dielectrophoresis (DEP) is the motion arising from the interaction of nonuniform electric fields and the induced electrical dipole in polarizable particles [1–5]. The standard electrical technique of electrophoretic separation works when suspended charged particles migrate under the influence of applied electric field. DEP has distinct advantages over this technique in that it can separate neutral particles as well, allowing the separation of particles without having to physiologically alter them; which gives minimum particle handling and no damage. DEP also typically uses microfabricated electrodes to generate highly nonuniform electric fields, which allows it to be performed locally, whereas electrophoretic separation is generally a long-range effect acting between two large external electrodes.

Due to the requirements for microfabrication, the localized nature of DEP, and the rapid growth of microfluidic Lab-on-a-Chip systems or μTAS in the past two decades in both research and commercial sectors [6–8], there has been a recent growth in the application of DEP to these areas. The first practical application of Lab-on-a-Chip was in fact on-chip CE [9] and with recent advances in the synthesis and the characterization of size-selected particles in the submicron and nanometer (colloidal) range, an investigation of their physical and chemical properties is now possible [10]. The capability to produce small scale devices allows the development of entirely novel experiments and chip-based analytical systems have been developed and applied to a variety of fields such as separation science, chemical production, DNA analysis, medical diagnostics, and environmental analysis.

This paper presents a brief review of DEP and its application to colloidal and nano particles. The application of this technique to the separation of particles is then discussed, again focusing on the activities in submicrometer particle separation. The paper then continues with the presentation of an innovative design for a double-sided aligned electrode array for the continuous flow-through separation of colloidal particles. Results of the application of the integrated microelectrode array in a microfluidic test device are then presented and discussed. The paper concludes with an estimation of the separation performance and efficiency.

1.2 Background

1.2.1 DEP and colloids

DEP is the movement of particles in nonuniform electric fields and the fundamental aspects of this behavior have been discussed in numerous publications [2, 11, 12]. The dielectrophoretic force on a spherical dielectric particle of radius a

Correspondence: Dr. Nicolas Green, Nano Group, School of Electronics and Computer Science, University of Southampton, Highfield, Southampton, SO17 1BJ, UK
E-mail: ng2@ecs.soton.ac.uk
Fax: +44-2380593029

Colour Online: See the article online to view Figs. 1–4 and 6 in colour.

suspended in a homogeneous dielectric medium, is

$$F_{\mathrm{DEP}} = \pi a^3 . \varepsilon_m \times \left[\frac{(\varepsilon_p - \varepsilon_m)(\varepsilon_p + 2\varepsilon_m) + \frac{1}{\omega^2}(\sigma_p - \sigma_m)(\sigma_p + 2\sigma_m)}{(\varepsilon_p + 2\varepsilon_m)^2 + \frac{1}{\omega^2}(\sigma_p + 2\sigma_m)^2} \right] . \nabla |E|^2 \quad (1)$$

where E is the electric field, ω is the angular frequency of the applied signal, ε is the permittivity, and σ is the conductivity of the particle (denoted by the p subscript) or medium (denoted by the m subscript).

Inspection of the DEP force expression shows three dependencies. First it depends on the volume of the particle, indicating that as the volume of the particle decreases, the force decreases proportionally. This is a critical issue with DEP of nanoscale particles. Second, it depends on the electrical properties of the particle and the fluid medium in a complex, frequency-dependent term enclosed by the square brackets. This term is referred to as the Clausius–Mossotti factor and it also affects the magnitude of the force to a slight degree but more importantly determines the direction of the DEP force. When the real part of this factor (expanded in the equation) is greater than zero, particles move toward strong electric field regions (referred to as positive DEP) and when the real part is less than zero, particles are repelled from strong field regions (negative DEP). This behavior allows DEP to discriminate between particle types, and therefore separate, based on differences in frequency dependency. The third dependency is that the force is proportional to the gradient of the electric field magnitude squared. This relationship is what allows DEP microsystems to be effective in the manipulation of nanoscale particles—rather than increase the voltage (which gives a squared increase in the force) to compensate for the reduction in the DEP force with particle volume, a reduction in the scale of the microsystem and the electrodes gives a cubed increase in force.

In a viscous fluid, all forces are heavily damped by viscous drag and the corresponding velocity v of the particle is simply proportional to the applied force with the proportionality given by the friction factor f:

$$v_{\mathrm{DEP}} = \frac{F_{\mathrm{DEP}}}{f} = \frac{\pi a^2}{6\pi\eta} . \varepsilon_m \times \left[\frac{(\varepsilon_p - \varepsilon_m)(\varepsilon_p + 2\varepsilon_m) + \frac{1}{\omega^2}(\sigma_p - \sigma_m)(\sigma_p + 2\sigma_m)}{(\varepsilon_p + 2\varepsilon_m)^2 + \frac{1}{\omega^2}(\sigma_p + 2\sigma_m)^2} \right] . \nabla |E|^2 \quad (2)$$

where the friction factor for a spherical particle in a fluid of viscosity η has been substituted. An important point to note is that the dielectrophoretic velocity is only proportional to the square of the particle radius.

The situation is further complicated by other forces in action on dielectric particles in suspension subjected to a nonuniform electric field. These include gravitation for larger and randomizing forces for smaller particles and a range of fluid flow forces, which could be augmented by the application of higher voltages and stronger electric fields. A quantitative comparison of the competing forces has been conducted by Ramos et al. (1998) [11], where the effect of non-DEP forces has been shown to be particularly pronounced for colloidal particles, due largely to the significance of Brownian motion and surface charge. The significance is such that DEP was perceived for long as able to generate motion of $\geq$1 μm particles for all other factors remaining constant. Accordingly, DEP applications were confined to microparticles. In several instances, DEP motion of cells and microorganisms was achieved with insignificant competition from fluid flow forces.

One critical point to note is that the design requirements for DEP devices for colloidal particles where Brownian motion dominate are substantially different than for larger, heavier particles where gravity dominates.

1.2.2 DEP of colloidal particles

It was the advent of semiconductor fabrication methods in DEP design that facilitated the extending of dielectrophoretic applications to colloidal particles. With electrode structures on the micro and nanometer scale, electric fields of sufficient strength to overcome randomizing effects were generated using voltages of modest magnitude, thereby avoiding unwanted electrothermal effects. Despite the presence of the enabling technology, the number of research groups having achieved DEP of colloidal particles remained small [13–21] until recently.

The majority of recent work related to colloidal particle DEP has involved particles with submicrometer dimensions across and micrometer-scale lengths. There are various reports on the immobilization, positioning, alignment, and assembly of DNA bundles [22–24], nanowires [25–29], nanorods [30, 31], and carbon nanotubes [32, 33], mainly for circuit and sensory functions. Among the few reports in recent years on DEP of colloidal particles, with all dimensions in the submicrometer range, are the DEP capture of virus particles using a probe array with nanoscale tips [34], the optically induced dielectrophoretic trapping and subsequent assembly into arrays of gold nanoparticles [35], the use of DEP in conjunction with hydrodynamic forces to enhance nanoparticle transfer for rapid biosensing [36], and DEP enhancement of protein detection in a silicon-nanowire biosensor [37].

1.2.3 Dielectrophoretic separation

DEP is particularly suitable as a label-free method of separating dielectric particles in suspension [38]. Simpler (yet with wide-ranging applicability) DEP separation procedures, predominantly visible in earlier applications of the technique,

rely on the distinction between positive and negative DEP to accumulate particles of higher/lower polarizability than the suspending medium in regions of higher/lower electric field strength. Castellated electrode structures, with well-defined regions of high and low field intensity, have been a favorite choice for DEP separations based on this principle. In a notable example, human breast cancer cells have been separated from blood and collected at the tips of castellated electrodes [39].

More sophisticated designs have relied on differences in DEP force magnitude (rather than sign only) to accomplish continuous-flow separation of multiple particle types from mixture suspensions. In an important development, DEP has been used in combination with sedimentation forces to add to the controllability of discriminating between different particles [40]. The technique, known as DEP-field-flow fractionation has been used for the separation of cell subpopulations from suspension [41, 42]. Based on differences in DEP spectra, i.e. variations of the dielectrophoretic force with electric field frequency, and through the combined action of dielectrophoretic and hydrodynamic forces, continuous-flow separation of viable (live) and nonviable (dead) cells has been achieved [43]. However, this technique relies on the relationship between gravity and DEP and would therefore not work on colloidal particles. More modern designs have used more advanced microfabrication methods to make sidewall electrodes [44] or to actually use channel designs and controlled liquids to make liquid electrodes [45] for flow-through separation applications.

There are abundant examples of DEP used alone or in conjunction with fluid flow forces to separate cells and other microparticles. However, as with DEP in general, few works have reported on dielectrophoretic separation of colloidal particles into distinct subpopulations. In related achievements, nanowires and nanotubes, which often have a mix of micrometer scale and submicrometer scale dimensions, have been separated through the effect of DEP (at times in conjunction with fluid flow forces) based on differences in particle shape or dielectric properties. A notable example has been the enrichment of metallic and/or semiconducting carbon nanotubes from mixture suspensions [46, 47]. Other examples include shape-dependent separation of ZnO particles using DEP and field-induced fluid flow [48] and the dielectrophoretic separation circulating from genomic DNA [49]. The few reports on dielectrophoretic separation of colloidal particles, with all dimensions on the submicrometer scale, include the DEP collection of viruses of two different types in regions of high/low electric field strength in a polynomial electrode geometry [50], the separation–using castellated electrodes–of 93 nm latex particles into distinct subpopulations characterized by their surface charge [51], size-dependent separation of 93 and 216 nm spherical particles from solution using the combined effect of dielectrophoretic and electrohydrodynamic forces [52] alongside examples of DEP separation of colloidal particles from their mixture with larger particles of micrometer dimensions [53, 54].

1.2.4 Dielectrophoretic separation using angled electrodes

Among the most effective electrode structures used for continuous-flow DEP separation are those that are angled with respect to the direction of suspension flow. Angled electrode structures have also been used as "funnels" to guide particle motion within a channel or as part of the function of a microsystem [55–59]. As DEP separators, angled electrode structures have been found favorable in their reliance on negative DEP for inducing forces of different strength on particles of different properties. The use of negative DEP assures no particle-electrode contact and is therefore minimally intrusive to the particles and minimally contaminating to the electrodes. The noncontact feature of DEP separation using angled electrodes makes them favorite candidates for bioparticle separation. Cell synchronization has been achieved based on size-dependent negative DEP force generated by angled electrodes and the technique found advantageous over conventional means in its noninvasiveness [60]. Using the same electrode arrangement, high-throughput separation of colloidal and micrometer biological particles from suspension [61–65] and the enrichment of rare bacteria expressing a specific surface marker from an excess of nontarget bacteria [66] have been achieved. Sequential angled electrodes have been used on top and bottom of a channel to sort cells prior to analysis [67]. In a similar work, the angle of electrodes with respect to the direction of fluid flow has been varied to facilitate DEP separation of particles of varying size, starting from 250 to 12 um [68]. Other related work using concepts similar to this include trapezoidal electrode arrays for continuous separation of microparticles [69], zig-zag paired electrode arrays in silicon and glass [70], high speed switched attenuators [71], a 3D fan-shaped electrode system [72], and a piece-wise curved array [73]. An elegant application of this type of design using imposed conductivity gradients has also been demonstrated [74].

The design tested in this paper uses angled electrodes consisting of two interdigitated arrays of chevron-shaped electrodes on top and bottom of a channel [75, 76]. The electrodes are not intended to act as barriers against particle motion, but to produce a cumulative displacement along the whole array with significantly less DEP force required per electrode. The advantage is particularly important for applications involving colloidal particles, where Brownian motion dominates their behavior. In addition, the particles are focused into the middle of the channel where the fluid moves fastest, improving sample throughput and reducing adhesion and contamination issues.

2 Materials and methods

The electrode array and the principle of operation are shown in schematic form in Fig. 1. The fabrication of these electrode arrays and their integration into microelectrode arrays has been fully described previously [77].

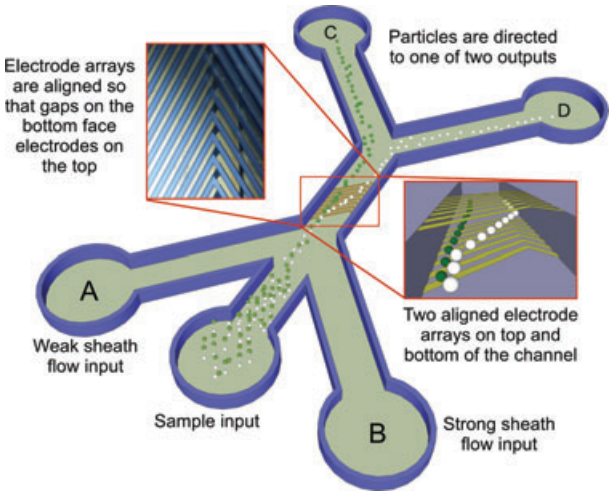

Figure 1. Schematic diagram of the principle of operation of the aligned microelectrodes array in the test microfluidic system. A sample containing particles is introduced through a port connector into a microfluidic channel. Hydrodynamic focusing is then used to focus the sample stream into a narrow beam of particles before entering the electrode array. In this case, the sheath flow rate on one side (port B) is greater than the other (port A), ensuring that the sample stream is positioned close to one side of the main channel and entering the microelectrode array at the top of the angled electrodes. The electrode array design consists of chevron-shaped interdigitated electrodes fabricated on the base of the channel with the electrode angling away from the channel wall to an apex near the far wall, with a second shorter angled section returning back up the channel. The electrodes are alternately connected to a potential signal and ground. A second mirror image microelectrode array on the top of the channel is aligned so that electrodes on the bottom face gaps on the top and vice-versa. As a heterogeneous mixture of particles passes through the array, particles that experience sufficient DEP force will deflect along the angled electrode and exit at different path at the end of the array, with the point in the chevron shape defining the exit position. In the test structure there are two exits for collection of particle samples, with the deflected particle type going to port D.

2.1 Electrode configuration

The electrode array used in this design were set at an angle to the microfluidic channel and hence the flow of particles. In addition, the electrodes were arranged with a chevron or "V" shape to define an exit point from the array at the apex of the chevron. In this work, as is shown in Fig. 1, the angle of the electrodes to the wall was 30°, with a corresponding inner angle at the apex of 60°. The width of the electrodes was approximately 19 μm and the gap between the electrodes was 25 μm. The electrode array was fabricated using photolithography on a pyrex substrate and the microelectrodes consisted of 200 nm of platinum on 20 nm of titanium as an adhesion layer. The electrodes are alternately connected to a bus-bar on either side of the array in a position insulated by the microfluidic channel wall and were designed to completely cross a channel of width 500 μm.

This microelectrode array is specifically designed for colloidal particles for which gravity is a negligible phenomenon. This requires the field to be symmetrical from top to bottom in the channel, so that the DEP force is predictable under the influence of Brownian motion [2]. As a result, two aligned arrays are required, one on top of the channel and one at the bottom, with a suitably low aspect ratio for the channel. The channel was fabricated by lithography of a Dry Film Resist, with a width of 500 μm and height of 40 μm, altering to 510 μm and height of 37 μm, following shrinkage during the curing process. The two electrode arrays are manually aligned under microscope with the electrode at the bottom facing the gap on the top and vice-versa. The top and bottom arrays are then slightly offset by 6 μm, measured using the microscope camera. A photographic inset of the fabricated microelectrodes can be seen in Fig. 1.

As shown schematically in the figure, particles entering the array will be deflected by the DEP force generated by the array. On both top and at bottom the electrodes are interdigitated, with an electrical signal and ground applied to alternate electrodes to generate a strong electric field and therefore DEP force. The use of two arrays top and bottom, ensures that the particles, when experiencing negative DEP are pushed into the vertical middle of the channel, where the fluid flow is fastest and therefore ensuring reproducible separation that occurs at a fast enough flow rate to be useful. Since the DEP force varies significantly with height above the electrodes and therefore the behavior of the particles is less predictable when they are free to move vertically, using two arrays to constrain the vertical movement will increase predictability. In addition, the symmetry of the field is essential for working with colloids, since Brownian motion and diffusion are symmetrical effects where gravity is not [2].

The arrays are also long, so that each electrode produces a slight deflection rather than stopping the particle against the flow, therefore allowing for smaller particles to be manipulated at low voltages. The use of negative DEP in the design also ensures that particles will be kept away from channel and electrode surfaces, which will prevent adhesion problems. The array is also therefore a flow-through separation system that can operate continuously.

2.2 Device and system design and operation

The microfluidic channel fabrication method has been described in a previous work [77] with the details of the microfluidic channel around the electrode array given in the previous section. Figure 1 shows a schematic of the operation of the test microfluidic system. The sample particle mixture stream is focused into a narrow beam by hydrodynamic focusing prior to entering the electrode array. The sheath flow is imbalanced in that the rate from one side (port B) is greater than the other (port A). This focuses the sample mixture to one side of the main channel so that it enters the microelectrode array at the top of the angled electrodes at the far side from the apex of the chevron electrodes. As a heterogeneous mixture of particles passes through the array, particles that experience sufficient DEP force will deflect along the angled

electrodes and exit at different path at the end of the array, with the point in the chevron shape defining the exit position. In the test structure there are two exits for collection of particle samples, which splits the output flow 50:50. The microfluidic chips were mounted inside a custom-designed microfluidic holder for the connection of external pumps [77] and the collection of separated samples from the outputs: ports C and D.

2.3 Experimental aspects

Fluorescent carboxylate-modified latex spheres were used in the experiment (yellow-green (505/515 nm) FluoSpheres, Molecular Probes, Eugene, OR. This type of particle are frequently used in assays, as a labeling index (beads per bacterial cell) or biomarkers [78, 79]. Fluorescent latex spheres contain high levels of various fluorescent dyes, making them easy to visualize, and are highly negatively charged, which ensures that they remain suspended. This makes them ideal flow tracers and practical particles for testing DEP systems. In this work, latex spheres with diameters of 2, 1, and 500 nm were used and suspended in test solutions of potassium chloride, KCl, with different concentrations to control the conductivity of the suspending medium. The SD in size for these particles was 5%. Mixtures of different particle sizes were prepared by washing down in different solutions to produce different samples.

As described in Fig. 2, the samples were injected continuously into the sample input with sheath flow solution with the same concentration of KCl into inputs A and B. The injection was controlled using syringe pumps and glass syringes: 250 μL Gastight #1725® by Hamilton-Bonaduz, Schweiz and 1000 μL MD-0100 from BASi with integrated controller pumps. The ratios of the different input flow streams were controlled by a single syringe pump controller.

Microfluidic channels were then observed under operation using a custom-designed fluorescence microscope [77] with a 10× Nikon Planfluor long working distance objective, which ensured that the whole depth of the channel was in focus. Signals were generated using a TTi (Thurlby Thandar Instruments) TGA1244 waveform generator with a GPIB interface and measured using an Agilent mixed signal oscilloscope 54641D. Video was recorded using a Panasonic 3CCD digital camera and recorded onto high definition digital video.

2.4 Image analysis

Experiments were recorded on high definition video with the signal generation and video capture hardware controlled by Matlab. Image analysis was then performed on video still frames using custom code written for Matlab, a block diagram of which is shown in Fig. 2, with an example still frame shown undergoing analysis for illustration purposes. NOTE: in all experiments performed on this design of array, the channel was arranged so that particles moved upwards in the video.

In the analysis, each video is reduced to a series of still images that are processed in sequence with individual particle tracked to ensure that individual particles are not counted multiple times. The still images are then converted to grayscale. This image is then thresholded with edge detection used to identify individual particles (black and white image in the figure). Intensity values from matching pixels in the grayscale image are then used to produce an intensity value for each particle. For the experiments in this paper, the

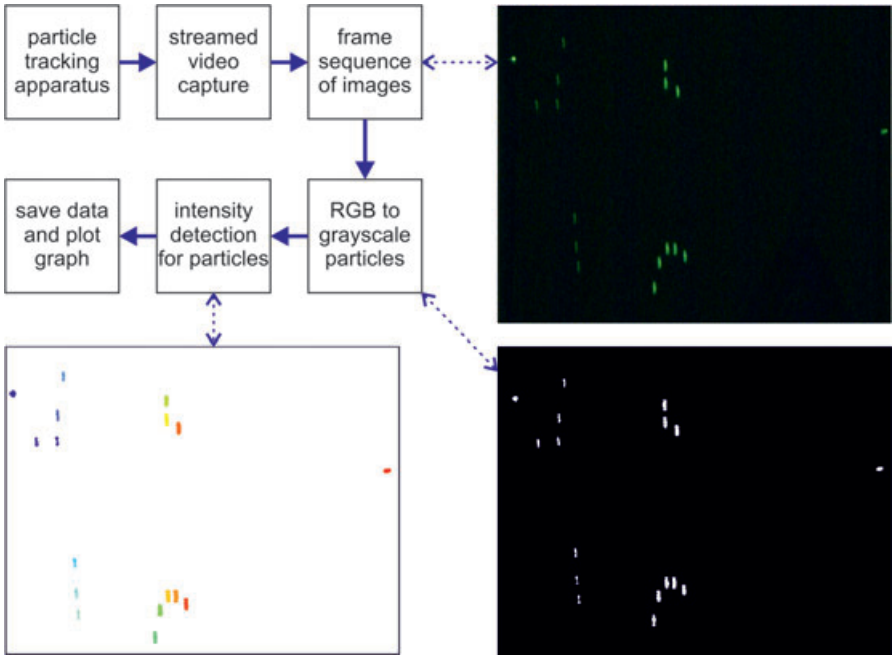

Figure 2. A block diagram showing the steps from capturing video of the flow of particles in a channel through analysis and data capture. The images show one still frame captured from a video, with particles moving upwards from bottom to top, followed by grayscale conversion and thresholding and finally labeling on the basis of size and intensity to detect different particles. In this case, final position of particles in the top 10% of the image (at a distance from the end of the microelectrode array) is used to determine the horizontal movement of particles across the channel by the DEP force.

final position of particles in the top 10% of the image (at a distance from the end of the microelectrode array) was then collected. The horizontal position of the particles in these images is then the horizontal exit position from the electrode array, from which the DEP deflection distance in the array can be calculated.

3 Results and discussion

Figure 3 shows typical experimental observations and data from the microfluidic channel and array. These data are for two sizes of particles (2 and 1 μm) suspended in KCl medium with a conductivity of 14.8 mS/m and an applied signal frequency of 1 MHz. The images here are constructed from several successive video frames by OR summing the pixels, to demonstrate the tracks of the individual particles up the channel. The particle density is very low (as seen in Fig. 2 and it was assumed that particles were sufficiently separated so that each could be seen independently. The sample flow rate was 0.1μL /min and the sheath flow rate was 0.5 μL/min.

Each image is paired with a scatter plot of arbitrary intensity versus distance from the left of the image in microns. The analyzed data of intensity (arbitrary unit) plotted against distance across the image (and therefore the channel), demonstrating that the large (brighter) particles have been displaced across the channel from the smaller (dimmer) particles. The four pairs (A–D) show the change in behavior as the applied voltage is increased from 12 volts peak-to-peak to 17 volts peak-to-peak. The scale of the image is indicated by the scale in the scatter plot; the width of the still image is 660 μm, and the channel width was 510 μm. The apex of array at the exit can be seen at the bottom of the images.

The lowest voltage, Fig. 3A, is the lowest voltage for which appreciable lateral movement of the 2 μm particles (the high intensity cluster) and therefore lateral separation from the 1 μm particles (low intensity cluster). As the voltage is increased, Fig. 3B and C, the 2 μm particle stream is deflected farther across the channel and broadens slightly. At the highest voltage, Fig. 3D, the 2 μm particle stream is deflected sufficiently for most of the particles to reach the array exit point at the apex. Those particles are then tightly focused into a stream exiting from the apex.

Figure 4 shows still video sequences and scatter plots of analyzed intensity data for the same two sizes of particles (2 and 1 μm) this time suspended in a KCl medium with conductivity 1.9 mS/m and again with an applied signal frequency of 1MHz. There are again four images and graphs shown for four different values of function of peak-to-peak voltage (Vpp): (i) 8.8, (ii), 11.5, (iii) 15.5, and (iv) 20 Vpp. Again, as the voltage is increased, lateral deflection of the 2 μm particle stream is observed that increases with applied voltage, separating from the 1 μm stream. It is also clear that the deflection is significantly smaller for the same applied voltage and frequency.

3.1 Theoretical analysis

This behavior is consistent with the theoretical description of DEP. In this system, with colloidal particles, the motion followed by the particles is that given by Eq. (2) with an appropriately simulated field-dependent term. The movement of the particles is therefore dependent on the square of the particle radius and the velocity exhibited by the 2 μm particles should be four times greater than that of the 1 μm particles. This dependency on size explains the difference between the observed movement of the larger particles and the smaller but also the large distribution of particle position. With a 5% SD in particle diameter, the variation in DEP velocity will be marked across the distribution of particle sizes (22% for one SD, 46% for two and so on.)

This microelectrode array works therefore within a window of voltages for a given particle type. Below a minimum voltage, no deflection is observed and above, the deflection rapidly increases to a maximum corresponding with the apex of the array, as indicated by the voltage squared dependency of the DEP force. The voltage would need to be sufficient to clearly separate the two streams of particles.

3.2 Analysis of separation

The deflection data were then analyzed in terms of physical separation of the two streams of particles. The image-processing algorithm gives horizontal position of the particle streams referenced to the sidewall. The mean position of the distribution of the two streams was then calculated and the difference in deflection between the two sizes of particles was then determined in order to give an estimation of the degree of separation of the two. Cumulative data for dozens of experiments and thousands of particle events are shown in Fig. 5, plotting the physical distance of separation of the two output streams (2 and 1 μm), from the mixture at the exit for the two medium conductivities: 1.9 and 14.8 mS/m and an applied voltage frequency of 1 MHz. Initially, the separation follows a voltage squared dependency as expected up to the voltage where the larger size of particle is exiting at the apex of the array.

At higher voltages the separation distance starts to decrease as the smaller particles are now being deflected by the applied field. This effect is more pronounced for the lower conductivity solution, which also resulted in the greatest distance of separation between the two streams. However, the variability in the data does not support a definitive conclusion about the difference between the two conductivities.

The separation results demonstrate complete stream separation of the two particle sizes in both media on a single pass through the device. The separation efficiency was tested independently by examining the output samples in an SEM facility used for biological testing. In the separated samples tested, cross contamination by the other particle size was not observed, indicating that the separation was close to 99.9%. However, these data were not considered absolutely

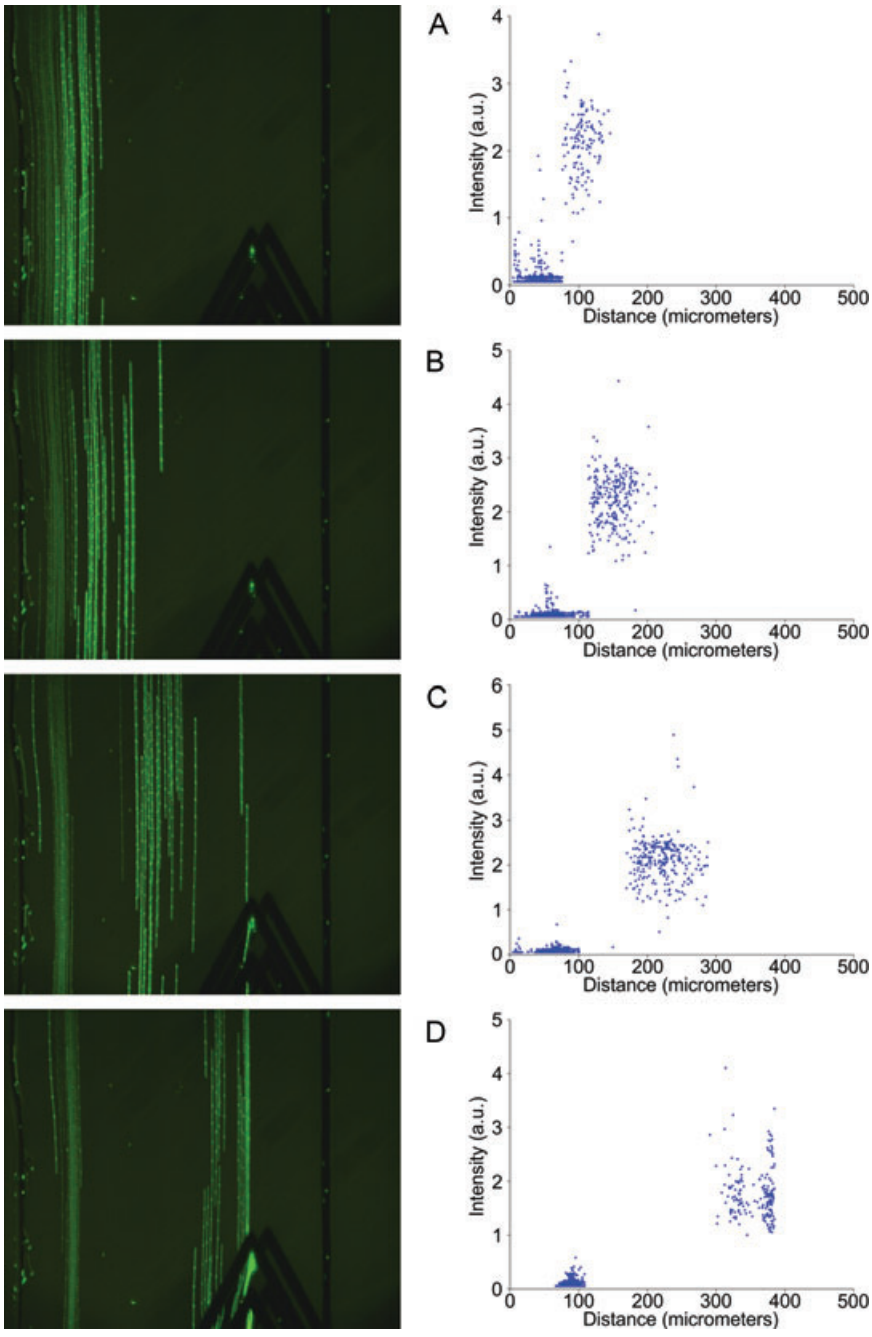

Figure 3. Still video sequences recorded of the motion of the particles at the exit of the array with particles moving from bottom to top. Images were taken from the video of separation with several subsequent images superimposed to show the path of the particles. Some of the particles have been deflected by the array, which can just be seen at the bottom of the image. Also shown are the analyzed data of intensity (arbitrary unit) plotted against distance across the image (and therefore the channel), demonstrating that the large (brighter) particles have been displaced across the channel from the smaller (dimmer) particles. These data are for two sizes of particles (2 and 1 μm) suspended in medium of 14.8 mS/m and frequency of 1 MHz as a function of peak-to-peak voltage (Vpp): (A) 12, (B) 14, (C) 15, and (D) 17 Vpp. The width of the still image is 660 μm and the channel width was 510 μm. The sample flow rate was 0.1 μL/min and the sheath flow rate was 0.5 μL/min.

conclusive as the recovery rate from the chip was only around 40% of the inputted sample.

4 Concluding remarks

The use of DEP for manipulation and separation has been reviewed, with particular attention to the application to colloidal and nanoparticles, indicating potential for a range of novel research opportunities. An innovative separation device has been demonstrated that uses negative DEP to achieve 99.9% noncontact separation of a mixture of colloidal particles. The separation method relies on the movement of one particle type, for which the dielectrophoretic force is stronger, away from the second particle type. In this case, this was the larger size of colloidal particle; with the smaller size remains unaffected by the force.

The use of two aligned microelectrode arrays on top and at bottom of the channel ensures that DEP force is stronger throughout the chamber, important for colloidal particles

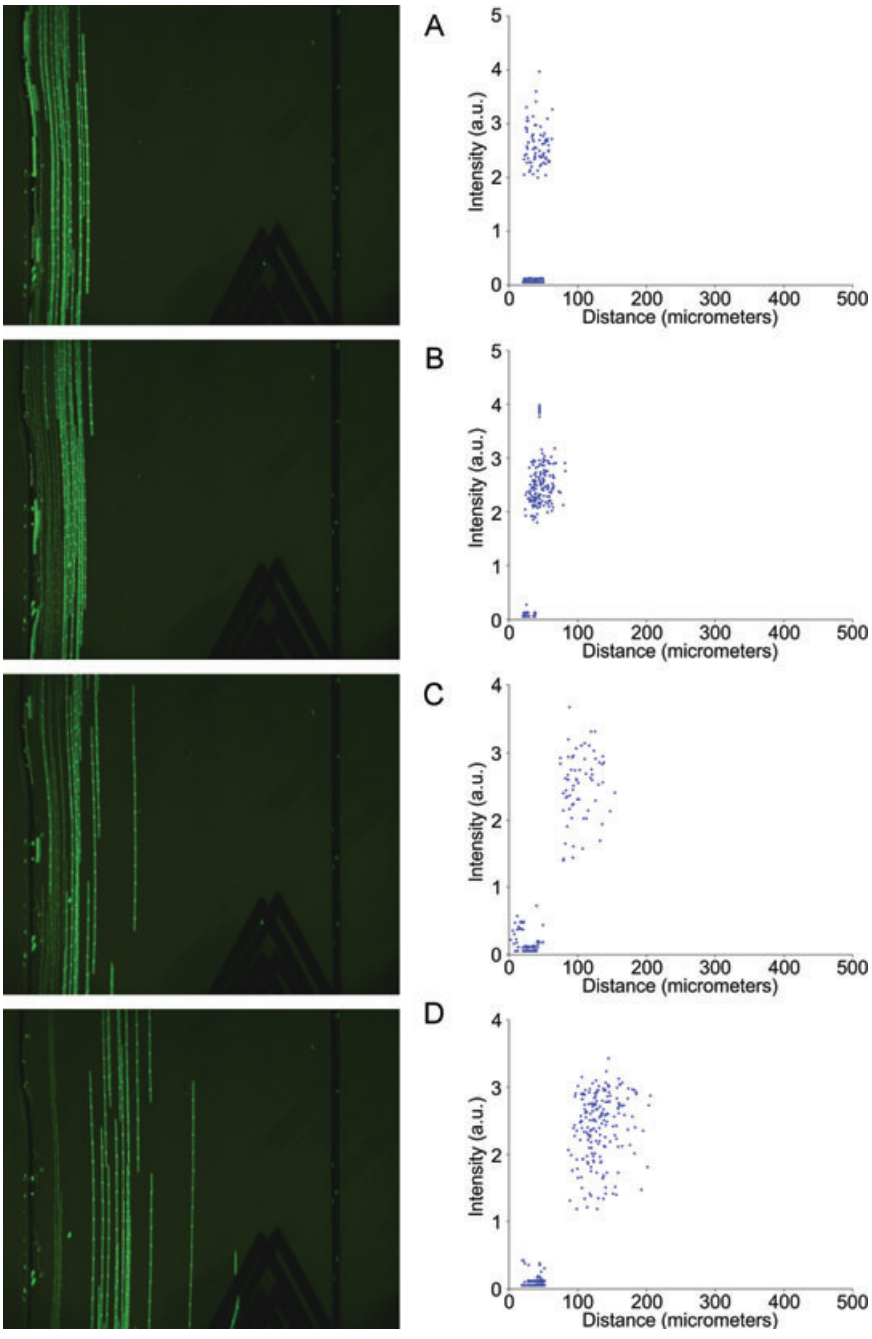

Figure 4. Still video sequences recorded of the motion of the particles at the exit of the array with particles moving from bottom to top. Images were taken from the video of separation with several subsequent images superimposed to show the path of the particles. Some of the particles have been deflected by the array, which can just be seen at the bottom of the image. Also shown are the analyzed data of intensity (arbitrary unit) plotted against distance across the image, demonstrating that the large (brighter) particles have been displaced across the channel from the smaller (dimmer) particles. These data are for two sizes of particles (2 and 1 μm) suspended in medium of 1.9 mS/m and frequency of 1 MHz as a function of peak-to-peak voltage (Vpp): (A) 8.8, (B) 11.5, (C) 15.5, and (D) 20 Vpp. The width of the still image is 660 μm and the channel width was 510 μm. The sample flow rate was 0.1 μL/min and the sheath flow rate was 0.5 μL/min.

where diffusion dominates and the system must be symmetrical. The separation method is continuous and flow-through and thus involves no contamination on the device (i.e. no fouling), ensuring longevity of operation. The separation is sensitive to medium conductivity and applied voltage, indicating that suitable conditions can be found to separate a wide range of particle types.

Future work with this electrode design will focus on complete characterization of the operation of the design and optimization of the physical characteristics in order to demonstrate its effectiveness on small nanoscale particles. Figure 6 shows a composite still image of the separation of 1 μm and 500 nm diameter spheres with an applied voltage of 30 Vpp. As expected, higher voltages allow the 1 μm particles to be deflected, however this level of potential difference would lead to complications for long-term operation in the form of electrochemical effects and damage to the electrodes. A superior solution would be to shrink the size of the electrode array and channel, or to determine if the angle of the electrodes is optimum for the separation of nanoparticles.

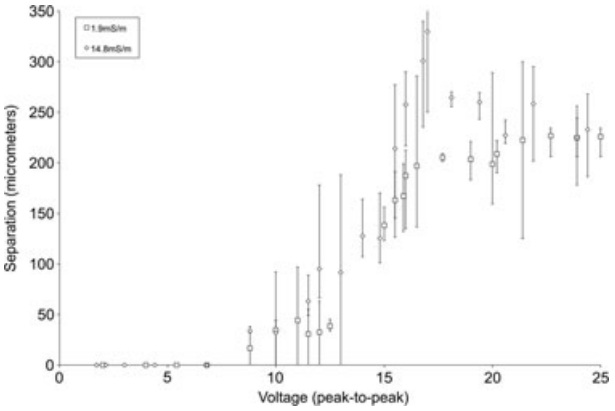

Figure 5. Analysis plots of physical distance of separation of the two output streams of particle 2 and 1 μm, from the mixture at the exit for a medium conductivity of 1.9 and 14.8 mS/m. These figures summarize a large number of experimental measurements of separation between the positions of the two particles as a function of voltage at 1 MHz. Initially, the separation follows a voltage squared dependency as expected up to the voltage where the larger size of particle is exiting at the apex of the array. At higher voltages the separation distance starts to decrease as the smaller particles are now being deflected by the applied field.

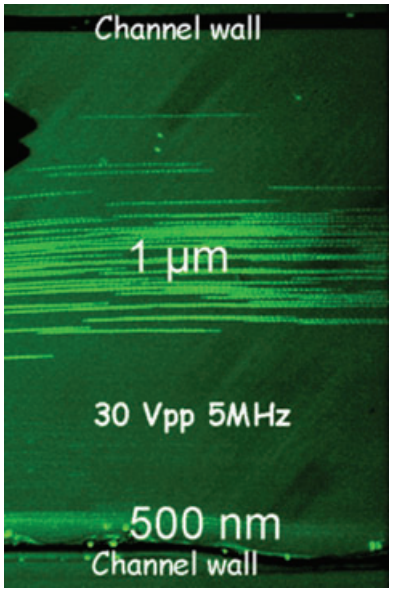

Figure 6. Composite still image of multiple video streams, showing particles exiting the microelectrode array. The input sample was a mix of 1 μm diameter and 500 nm diameter latex spheres. The applied signal was 30 Vpp at a frequency of 5 MHz. The 1 μm particle stream is deflected by the array away from the 500 nm stream near the wall.

The authors would like to acknowledge the Ministry of Higher Education and University Putra Malaysia, Malaysia for the award of a studentship to Nurul Amziah Md. Yunus and the Royal Academy of Engineering, United Kingdom for support to NG Green.

There are no financial or commercial conflicts arising from the publication of this material.

5 References

[1] Pohl, H. A., *J. Appl. Phys.* 1951, *22*, 869–871.

[2] Morgan, H., Green, N. G., *AC Electrokinetics: Colloids and Nanoparticles*, Research Studies Press, Baldock, UK, 2003.

[3] Pethig, R., *Biomicrofluidics* 2010, *4*, 022811.

[4] Cetin B, Li, D., *Electrophoresis* 2011, *32*, 2410–2427.

[5] Gagnon, Z.R., *Electrophoresis* 2011, *32*, 2466–2487.

[6] Manz, A., Graber, N., Widmer, H. M., *Sens. Actuators B* 1990, *1*, 244–248.

[7] Reyes, D. R., Iossifidis, D., Auroux, P. A., Manz, A., *Anal. Chem.* 2002, *74*, 2623–2636.

[8] Haeberle, S., Zengerle, R., *Lab Chip* 2007, *7*, 1094–1110.

[9] Manz, A., Harrison, D. J., Verpoorte, E. M. J., Fettinger, J. C., Paulus, A., Lüdi, H., Widmer, H. M., *J. Chromatogr.* 1992, *593*, 253–258.

[10] Shirinyan, A. S., Wautelet, M., *Nanotechnology* 2004, *15*, 1720–1731.

[11] Ramos, A., Morgan, H., Green, N. G., Castellanos, A., *J. Phys. D Appl. Phys.* 1998, *31*, 2338–2353.

[12] Jones, T. B., *Electromechanics of Particles*, Cambridge University Press, Cambridge, UK, 1995.

[13] Washizu, M., Suzuki, S., Kurosawa, O., Nishizaka, T., Shinohara, T., *IEEE Trans. Ind. Appl.* 1994, *30*, 835–843.

[14] Washizu, M., Kurosawa, O., Arai, I., Suzuki, S., Shimamoto, N., *IEEE Trans. Ind. Appl.* 1995, *31*, 447–456.

[15] Markx, G. H., Pethig, R., Rousselet, J., *J. Phys. D Appl. Phys.* 1997, *30*, 2470–2477.

[16] Brown, A. P., Milner, K. R., Allsopp, D. W. E., Betts, W. B., *Electron. Lett.* 1998, *34*, 1934–1936.

[17] Zheng, L. F., Brody, J. P., Burke, P. J., *Biosens. Bioelectron.* 2004, *20*, 606–619.

[18] Morgan, H., Green, N. G., *J. Electrostatics* 1997, *42*, 279–293.

[19] Green, N.G., Morgan, H., Milner, J. J., *J. Biochem. Biophys. Methods* 1997, *35*, 89–102.

[20] Green, N. G., Morgan, H., *J. Phys. Chem. B* 1999, *103*, 41–50.

[21] Kuzyk, A., *Electrophoresis* 2011, *32*, 2307–2312.

[22] Yamahata, C., Collard, D., Legrand, B., Takekawa, T., Kumemura, M., Hashiguchi, G., Fujita, H., *J. Microelectromech. Syst.* 2008, *17*, 623–631.

[23] Chou, C.-F., Tegenfeldt, J. O., Bakajin, O., Chan, S. S., Cox, E. C., Darnton, N., Duke, T., Austin, R. H., *J. Biophys.* 2002, *83*, 2170–2179.

[24] Camacho-Alanis, F., Gan, L., Ros, A., *Sens. Actutators B Chem.* 2012, *173*, 668–675.

[25] Kim, T. H., Lee, S. Y., Cho, N. K., Seong, H. K., Choi, H. J., Jung, S. W., Lee, S. K., *Nanotechnology* 2006, *17*, 3394–3399.

[26] Freer, E. M., Grachev, O., Duan, X., Martin, S., Stumbo, D. P., *Nat. Nanotechnol.* 2010, *5*, 525–530.

[27] Lee, S.-Y., Umar, A., Suh, D.-I., Park, J.-E., Hahn, Y.-B., Ahn, J.-Y., Lee, S.-K., *Physica E* 2008, *40*, 866–872.

[28] Simpkins, B. S., McCoy, K. M., Whitman, L. J., Pehrsson, P. E., *Nanotechnology* 2007, *18*, 355301.

[29] Suehiro, J., Nakagawa, N., Hidaka, S.-I., Ueda, M., Imasaka, K., Higashihata, M., Okada, T., Hara, M., *Nanotechnology* 2006, *17*, 2567–2573.

[30] Jiang, K., Liu, W., Wan, L., Zhang, J., *Sens. Actutators B Chem.* 2008, *134*, 79–88.

[31] Evoy, S., DiLello, N., Deshpande, V., Narayanan, A., Liu, H., Riegelman, M., Martin, B. R., Hailer, B., Bradley, J.-C., Weiss, W., Mayer, T.S., Gogotsi, Y., Bau, H.H., Mallouk, T.E., Raman, S., *Microelectron. Eng.* 2004, *75*, 31–42.

[32] Stokes, P., Khondaker, S. I., *Appl. Phys. Lett.* 2010, *96*, 083110.

[33] Fung, C. K. M., Wong, V. T. S., Chan, R. H. M., Li, W. J., *IEEE Trans. Nanotechnol.* 2004, *3*, 395–403.

[34] Park, K., Akin, D., Bashir, R., *Biomed. Microdevices* 2007, *9*, 877–883.

[35] Miao, X., Lin, L. Y., *Opt. Lett.* 2007, *32*, 295–297.

[36] Fatoyinbo, H. O., Hoettges, K. F., Reddy, S. M., Hughes, M. P., *Biosens. Bioelectron.* 2007, *23*, 225–232.

[37] Gong, J.-R., *Small* 2010, *6*, 967–973.

[38] Gascoyne, P. R. C., Vykoukal, J., *Electrophoresis* 2002, *23*, 1973–1983.

[39] Becker, F. F., Wang, X. B., Huang, Y., Pethig, R., Vykoukal, J., Gascoyne, P. R. C., *Proc. Natl. Acad. Sci. USA* 1995, *92*, 860–864.

[40] Huang, Y., Wang, X., Becker, F., Gascoyne, P. R. C., *Biophys. J.* 1997, *73*, 1118–1129.

[41] Yang, J., Huang, Y., Wang, X.-B., Becker, F. F., Gascoyne, P. R. C., *Anal. Chem.* 1999, *71*, 911–918.

[42] Wang, X.-B., Yang, J., Huang, Y., Vykoukal, J., Becker, F. F., Gascoyne, P. R. C., *Anal. Chem.* 2000, *72*, 832–839.

[43] Doh, I., Cho, Y.-H., *Sens. Actuators A Phys.* 2005, *121*, 59–65.

[44] Wang, L., Flanagan, L. A., Jeon, N. L., Monuki, E., Lee, A. P., *Lab Chip* 2007, *7*, 1114–1120.

[45] Demierre, N., Braschler, T., Linderholm, P., Seger, U., Lintel, H., Renaud, P., *Lab Chip* 2007, *7*, 355–365.

[46] Krupke, R., Hennrich, F., Löhneysen, H. v, Kappes, M. M., *Science* 2003, *301*, 344–347.

[47] Shin, D. H., Kim, J.-E., Shim, H. C., Song, J.-W., Yoon, J.-H., Kim, J., Jeong, S., Kang, J., Baik, S., Han, C. S., *Nano. Lett.* 2008, *8*, 4380–4385.

[48] Riahifar, R., Marzbanrad, E., Raissi, B., Zamani, C., Kazemzad, M., and Aghaei, A., *Mater. Lett.* 2011, *65*, 632–635.

[49] Yeo, W., Chung, L., Yaling, L., Lee, K.-H., in: Razeghi, M., Mohseni, H. (Eds.) *Proc. SPIE* 2008, *7035*, 70350N-1.

[50] Morgan, H., Hughes, M. P., Green, N. G., *Biophys. J.* 1999, *77*, 516–525.

[51] Green, N. G., Morgan, H., *J. Phys. D Appl. Phys.* 1997, *30*, L41–L44.

[52] Green, N. G., Morgan, H, *J. Phys. D Appl. Phys.* 1998, *31*, L25–L30.

[53] Krishnan, R., Dehlinger, D. A., Gemmen, G. J., Mifflin, R. L., Esener, S. C., Heller, M., *J. Electrochem. Commun.* 2009, *11*, 1661–1666.

[54] Chávez-Santoscoy, A. V., Baylon-Cardiel, J. L., Moncada-Hernández, H., Lapizco-Encinas, B. H., *Sep. Sci. Technol.* 2011, *46*, 384–394.

[55] Fiedler, S., Shirley, S. G., Schnelle, T., Fuhr, G., *Anal. Chem.* 1998, *70*, 1909–1915.

[56] Müller, T., Gradl, G., Howitz, S., Shirley, S., Schnelle, T., Fuhr, G., *Biosens. Bioelectron.* 1999, *14*, 247–256.

[57] Alazzam, A., Stiharu, I., Bhat, R., Meguerditchian, A.-N., *Electrophoresis* 2011, *32*, 1327–1336.

[58] Bessette, P. H., Hu, X., Soh, H. T., Daugherty, P. S., *Anal. Chem.* 2007, *79*, 2174–2178.

[59] Seger, U., Gawad, S., Johann, R., Bertsch, A., Renaud, P., *Lab Chip* 2004, *4*, 148–151.

[60] Kim, U., Shu, C.-W., Dane, K. Y., Daugherty, P. S., Wang, J. Y. J., Soh, H. T., *Proc. Natl. Acad. Sci. USA* 2007, *104*, 20708–20712.

[61] Dehlinger, D. A., Rose, K. A., Shusteff, M., Bailey, C. G., Mariella Jr., R. P., *US Patent* No. 0259745, October 27, 2011, USA.

[62] Din, N. D., Liu, C. H., *Third International Conference on the Development of Biomedical Engineering, Ho Chi Minh City*, Vietnam 2010, 308–311.

[63] Kim, U., Soh, H. T., *Lab Chip* 2009, *9*, 2313–2318.

[64] Kim, U., Qian, J., Kenrick, S. A., Daugherty, P. S., Soh, H. T., *Anal. Chem.* 2008, *80*, 656–661.

[65] Kralj, J. G., Lis, M. T. W., Schmidt, M. A., Jensen, K. F., *Anal. Chem.* 2006, *78*, 5019–5025.

[66] Hu, X., Bessette, P. H., Qian, J., Meinhart, C. D., Daugherty, P. S., Soh, H. T., *Proc. Natl. Acad. Sci. USA* 2005, *102*, 15757–15761.

[67] Muratore, M., Srsen, V., Waterfall, M., Downes, A., Pethig, R., *Biomicrofluidics* 2012, *6*, 034113.

[68] Dürr, M., Kentsch, J., Müller, T., Schnelle, T., Stelzle, M., *Electrophoresis* 2003, *24*, 722–731.

[69] Choi, S., Park, J. K., *Lab. Chip.* 2005, *5*, 1161–1167.

[70] Chen, D. F., Du, H., Li, W. H., *J. Micromech. Microeng.* 2006, *16*, 1162–1169.

[71] Nieuwenhuis, J. H., Jachimowicz, A., Svasek, P., Vellekoop, M. J., *Proc. of IEEE Sensors* 2004, *1*, 64–67.

[72] Park, J., Kim, B., Choi, S. K., Hong, S., Lee, S. H., Lee, K. I., *Lab Chip* 2005, *5*, 1264–1270.

[73] Han, K. H., Han, S. I., Frazier, A. B., *Lab Chip* 2009, *9*, 2958–2964.

[74] Vahey, M. D., Voldman, J., *Anal. Chem.* 2008, *80*, 3135–343.

[75] Yunus, N. A. M., Green, N. G., *J. Phys. Conf. Ser.* 2008, *142*, 012068.

[76] Yunus, N. A. M., Green, N. G., *Twelfth International Conferences on Miniaturized Systems for Chemistry and Life Sciences*, San Diego, CA, USA 2008, 1447–1449.

[77] Yunus, N. A. M., Green, N. G., *Microsyst. Technol.* 2010, *16*, 2099–2107.

[78] Wang, Y. C., Han, J., *Lab Chip* 2008, *8*, 392–394.

[79] Liu, G., Wang, J., Wu, H., Lin, Y., *Electroanalysis* 2007, *19*, 777–785.

